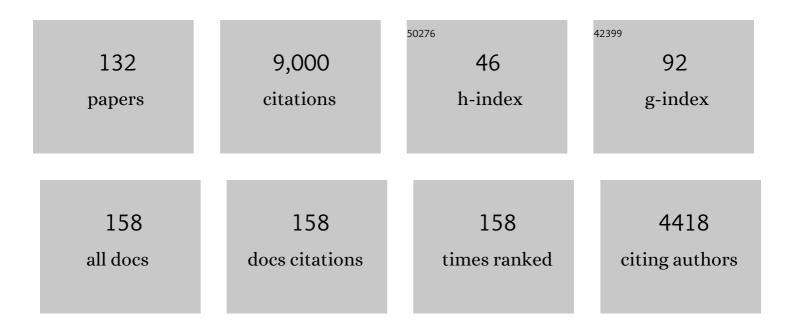
## Xiaohui Yuan

List of Publications by Year in descending order

Source: https://exaly.com/author-pdf/3779924/publications.pdf Version: 2024-02-01



#	Article	IF	CITATIONS
1	Seismic Images of Crust and Upper Mantle Beneath Tibet: Evidence for Eurasian Plate Subduction. Science, 2002, 298, 1219-1221.	12.6	570
2	The rapid drift of the Indian tectonic plate. Nature, 2007, 449, 894-897.	27.8	391
3	Seismic Evidence for a Detached Indian Lithospheric Mantle Beneath Tibet. Science, 1999, 283, 1306-1309.	12.6	371
4	The elusive lithosphere–asthenosphere boundary (LAB) beneath cratons. Lithos, 2009, 109, 1-22.	1.4	365
5	Lithospheric and upper mantle structure of southern Tibet from a seismological passive source experiment. Journal of Geophysical Research, 1997, 102, 27491-27500.	3.3	338
6	Subduction and collision processes in the Central Andes constrained by converted seismic phases. Nature, 2000, 408, 958-961.	27.8	337
7	The boundary between the Indian and Asian tectonic plates below Tibet. Proceedings of the National Academy of Sciences of the United States of America, 2010, 107, 11229-11233.	7.1	332
8	Rejuvenation of the lithosphere by the Hawaiian plume. Nature, 2004, 427, 827-829.	27.8	233
9	Evidence from Earthquake Data for a Partially Molten Crustal Layer in Southern Tibet. Science, 1996, 274, 1692-1694.	12.6	226
10	Moho topography in the central Andes and its geodynamic implications. Earth and Planetary Science Letters, 2002, 199, 389-402.	4.4	222
11	Seismic signature of the collision between the east Tibetan escape flow and the Sichuan Basin. Earth and Planetary Science Letters, 2010, 292, 254-264.	4.4	203
12	TheSreceiver functions: synthetics and data example. Geophysical Journal International, 2006, 165, 555-564.	2.4	191
13	Imaging the colliding Indian and Asian lithospheric plates beneath Tibet. Journal of Geophysical Research, 2006, 111, n/a-n/a.	3.3	186
14	Mapping the Hawaiian plume conduit with converted seismic waves. Nature, 2000, 405, 938-941.	27.8	174
15	Tearing of the Indian lithospheric slab beneath southern Tibet revealed by SKS-wave splitting measurements. Earth and Planetary Science Letters, 2015, 413, 13-24.	4.4	171
16	Seismic Detection and Characterization of the Altiplano-Puna Magma Body, Central Andes. Pure and Applied Geophysics, 2003, 160, 789-807.	1.9	161
17	Seismic imaging of subducting continental lower crust beneath the Pamir. Earth and Planetary Science Letters, 2013, 375, 101-112.	4.4	158
18	Geometry of the Pamirâ€Hindu Kush intermediateâ€depth earthquake zone from local seismic data. Journal of Geophysical Research: Solid Earth, 2013, 118, 1438-1457.	3.4	156

Χιαομυι Υυαν

#	Article	IF	CITATIONS
19	Seismic receiver functions and the lithosphere–asthenosphere boundary. Tectonophysics, 2012, 536-537, 25-43.	2.2	150
20	Deep India meets deep Asia: Lithospheric indentation, delamination and break-off under Pamir and Hindu Kush (Central Asia). Earth and Planetary Science Letters, 2016, 435, 171-184.	4.4	148
21	The lithosphere-asthenosphere boundary in the Tien Shan-Karakoram region from S receiver functions: Evidence for continental subduction. Geophysical Research Letters, 2005, 32, n/a-n/a.	4.0	147
22	Seismic imaging of a convergent continental margin and plateau in the central Andes (Andean) Tj ETQq0 0 0 rgBT	/9yerlock	10 Tf 50 62 128
23	The lithosphere–asthenosphere boundary in the North-West Atlantic region. Earth and Planetary Science Letters, 2005, 236, 249-257.	4.4	126
24	Receiver functions in northeast China – implications for slab penetration into the lower mantle in northwest Pacific subduction zone. Earth and Planetary Science Letters, 2003, 216, 679-691.	4.4	120
25	The lithosphere-asthenosphere boundary beneath the western United States. Geophysical Journal International, 2007, 170, 700-710.	2.4	117
26	Crustal and uppermost mantle velocity structure along a profile across the Pamir and southern Tien Shan as derived from project TIPAGE wide-angle seismic data. Geophysical Journal International, 2012, 188, 385-407.	2.4	113
27	Seismotectonics of the Pamir. Tectonics, 2014, 33, 1501-1518.	2.8	108
28	An S receiver function analysis of the lithospheric structure in South America. Geophysical Research Letters, 2007, 34, .	4.0	96
29	Deep burial of Asian continental crust beneath the Pamir imaged with local earthquake tomography. Earth and Planetary Science Letters, 2013, 384, 165-177.	4.4	91
30	Seismic evidence for stratification in composition and anisotropic fabric within the thick lithosphere of Kalahari Craton. Geochemistry, Geophysics, Geosystems, 2013, 14, 5393-5412.	2.5	85
31	Receiver function study of the Hellenic subduction zone: imaging crustal thickness variations and the oceanic Moho of the descending African lithosphere. Geophysical Journal International, 2003, 155, 733-748.	2.4	82
32	A detailed receiver function image of the upper mantle discontinuities in the Japan subduction zone. Earth and Planetary Science Letters, 2000, 183, 527-541.	4.4	79
33	Evidence for a missing crustal root and a thin lithosphere beneath the Central Alborz by receiver function studies. Geophysical Journal International, 2009, 177, 733-742.	2.4	79
34	Magmatic underplating and crustal growth in the Emeishan Large Igneous Province, SW China, revealed by a passive seismic experiment. Earth and Planetary Science Letters, 2015, 432, 103-114.	4.4	78
35	Teleseismic tomography of the southern Puna plateau in Argentina and adjacent regions. Tectonophysics, 2013, 586, 65-83.	2.2	76
36	Thickness of the lithosphere beneath Turkey and surroundings from S-receiver functions. Solid Earth, 2015, 6, 971-984.	2.8	72

3

Χιαομυι Υυαν

#	Article	IF	CITATIONS
37	The Moho beneath western Tibet: Shear zones and eclogitization in the lower crust. Earth and Planetary Science Letters, 2014, 408, 370-377.	4.4	71
38	USArray Receiver Function Images of the Lithosphere-Asthenosphere Boundary. Seismological Research Letters, 2012, 83, 486-491.	1.9	68
39	Seismic Images of the Biggest Crash on Earth. Science, 2010, 329, 1479-1480.	12.6	66
40	Lithospheric thickness beneath the Dabie Shan, central eastern China from <i>S</i> receiver functions. Geophysical Journal International, 2006, 166, 1363-1367.	2.4	64
41	Mapping crustal structure beneath southern Tibet: Seismic evidence for continental crustal underthrusting. Gondwana Research, 2015, 27, 1487-1493.	6.0	63
42	Detailed Configuration of the Underthrusting Indian Lithosphere Beneath Western Tibet Revealed by Receiver Function Images. Journal of Geophysical Research: Solid Earth, 2017, 122, 8257-8269.	3.4	54
43	Seismic study of upper mantle and transition zone beneath hotspots. Physics of the Earth and Planetary Interiors, 2003, 136, 79-92.	1.9	52
44	Receiver function analysis of the North American crust and upper mantle. Geophysical Journal International, 2002, 150, 91-108.	2.4	49
45	Crustal thickness estimation beneath the southern central Andes at 30°S and 36°S from <i>S</i> wave receiver function analysis. Geophysical Journal International, 2008, 174, 249-254.	2.4	48
46	Receiver function images from the Moho and the slab beneath the Altiplano and Puna plateaus in the Central Andes. Geophysical Journal International, 2009, 177, 296-308.	2.4	48
47	Seismic evidence for widespread serpentinized forearc mantle along the Mariana convergence margin. Geophysical Research Letters, 2008, 35, .	4.0	47
48	Depthâ€variant azimuthal anisotropy in Tibet revealed by surface wave tomography. Geophysical Research Letters, 2015, 42, 4326-4334.	4.0	46
49	Moho geometry and upper mantle images of northeast India. Geophysical Research Letters, 2005, 32, n/a-n/a.	4.0	44
50	Insight into the subducted Indian slab and origin of the Tengchong volcano in SE Tibet from receiver function analysis. Earth and Planetary Science Letters, 2018, 482, 567-579.	4.4	44
51	Central Andean mantle and crustal seismicity beneath the Southern Puna plateau and the northern margin of the Chileanâ€Pampean flat slab. Tectonics, 2014, 33, 1636-1658.	2.8	42
52	The Crust in the Pamir: Insights From Receiver Functions. Journal of Geophysical Research: Solid Earth, 2019, 124, 9313-9331.	3.4	42
53	Seismic monitoring of the Indian Ocean tsunami. Geophysical Research Letters, 2005, 32, .	4.0	41
54	Receiver function summation without deconvolution. Geophysical Journal International, 2010, 180, 1223-1230.	2.4	41

Χιαοήμι Υμάν

#	Article	IF	CITATIONS
55	ls the Asian lithosphere underthrusting beneath northeastern Tibetan Plateau? Insights from seismic receiver functions. Earth and Planetary Science Letters, 2015, 428, 172-180.	4.4	41
56	Deep origin of the Hawaiian tilted plume conduit derived from receiver functions. Geophysical Journal International, 2006, 166, 767-781.	2.4	40
57	Upper mantle and lithospheric heterogeneities in central and eastern Europe as observed by teleseismic receiver functions. Geophysical Journal International, 2008, 174, 351-376.	2.4	40
58	More constraints to determine the seismic structure beneath the Central Andes at 21°S using teleseismic tomography analysis. Journal of South American Earth Sciences, 2008, 25, 22-36.	1.4	40
59	Structure of the crust and the lithosphere beneath the southern Puna plateau from teleseismic receiver functions. Earth and Planetary Science Letters, 2014, 385, 1-11.	4.4	40
60	A 3D shear-wave velocity model of the upper mantle beneath China and the surrounding areas. Tectonophysics, 2014, 633, 193-210.	2.2	40
61	The Hindu Kush slab break-off as revealed by deep structure and crustal deformation. Nature Communications, 2021, 12, 1685.	12.8	39
62	High-resolution image of the geometry and thickness of the subducting Nazca lithosphere beneath northern Chile. Journal of Geophysical Research, 2011, 116, .	3.3	38
63	Complex structure of upper mantle beneath the Yadong-Gulu rift in Tibet revealed by S-to-P converted waves. Earth and Planetary Science Letters, 2020, 531, 115954.	4.4	37
64	Anisotropic lowâ€velocity lower crust beneath the northeastern margin of <scp>T</scp> ibetan <scp>P</scp> lateau: Evidence for crustal channel flow. Geochemistry, Geophysics, Geosystems, 2015, 16, 4223-4236.	2.5	35
65	Normal faulting from simple shear rifting in South Tibet, using evidence from passive seismic profiling across the Yadong-Gulu Rift. Tectonophysics, 2013, 606, 178-186.	2.2	34
66	A ubiquitous lowâ€velocity layer at the base of the mantle transition zone. Geophysical Research Letters, 2014, 41, 836-842.	4.0	32
67	Seismic observation of narrow plumes in the oceanic upper mantle. Geophysical Research Letters, 2003, 30, .	4.0	30
68	Continental lithospheric subduction and intermediate-depth seismicity: Constraints from S-wave velocity structures in the Pamir and Hindu Kush. Earth and Planetary Science Letters, 2018, 482, 478-489.	4.4	29
69	Crustal thickness and <i>V<sub>p</sub></i> / <i>V<sub>s</sub></i> ratio in NW Namibia from receiver functions: Evidence for magmatic underplating due to mantle plumeâ€crust interaction. Geophysical Research Letters, 2015, 42, 3330-3337.	4.0	27
70	Sharp Lateral Moho Variations Across the SE Tibetan Margin and Their Implications for Plateau Growth. Journal of Geophysical Research: Solid Earth, 2020, 125, e2019JB018117.	3.4	27
71	Intracontinental deformation of the Tianshan Orogen in response to India-Asia collision. Nature Communications, 2022, 13, .	12.8	27
72	The lithosphere-asthenosphere boundary observed with USArray receiver functions. Solid Earth, 2012, 3, 149-159.	2.8	26

XIAOHUI YUAN

#	Article	IF	CITATIONS
73	Study of the lithospheric and upper-mantle discontinuities beneath eastern Asia by SS precursors. Geophysical Journal International, 2010, 183, 252-266.	2.4	25
74	Scandinavia: A former Tibet?. Geochemistry, Geophysics, Geosystems, 2013, 14, 4479-4487.	2.5	25
75	Velocity structure beneath the southern Puna plateau: Evidence for delamination. Geochemistry, Geophysics, Geosystems, 2013, 14, 4292-4305.	2.5	25
76	Tearing of the mantle lithosphere along the intermediateâ€depth seismicity zone beneath the Gibraltar Arc: The onset of lithospheric delamination. Geophysical Research Letters, 2017, 44, 4027-4035.	4.0	25
77	Receiver function images of the central Chugoku region in the Japanese islands using Hi-net data. Earth, Planets and Space, 2005, 57, 271-280.	2.5	24
78	Crustal structure of southern Madagascar from receiver functions and ambient noise correlation: Implications for crustal evolution. Journal of Geophysical Research: Solid Earth, 2017, 122, 1179-1197.	3.4	24
79	Detailed Moho variations under Northeast China inferred from receiver function analyses and their tectonic implications. Physics of the Earth and Planetary Interiors, 2020, 300, 106448.	1.9	24
80	New insights into the structural elements of the upper mantle beneath the contiguous United States from <i>S</i> -to- <i>P</i> converted seismic waves. Geophysical Journal International, 2020, 222, 646-659.	2.4	24
81	Seismological Studies of the Central and Southern Andes. , 2006, , 443-457.		24
82	Delamination of southern Puna lithosphere revealed by body wave attenuation tomography. Journal of Geophysical Research: Solid Earth, 2014, 119, 549-566.	3.4	23
83	Seismic anisotropy of the lithosphere and asthenosphere beneath southern Madagascar from teleseismic shear wave splitting analysis and waveform modeling. Journal of Geophysical Research: Solid Earth, 2016, 121, 6627-6643.	3.4	22
84	A STEP fault in Central Betics, associated with lateral lithospheric tearing at the northern edge of the Gibraltar arc subduction system. Earth and Planetary Science Letters, 2018, 486, 32-40.	4.4	22
85	Lateral Moho variations and the geometry of the Main Himalayan Thrust beneath the Nepal Himalayan orogen revealed by teleseismic receiver functions. Geophysical Journal International, 2018, 214, 1004-1017.	2.4	22
86	Detection of a new sub-lithospheric discontinuity in Central Europe with S-receiver functions. Tectonophysics, 2017, 700-701, 19-31.	2.2	21
87	Full Waveform Inversion Beneath the Central Andes: Insight Into the Dehydration of the Nazca Slab and Delamination of the Backâ€Arc Lithosphere. Journal of Geophysical Research: Solid Earth, 2021, 126, e2021JB021984.	3.4	21
88	Structure of the upper mantle in the north-western and central United States from USArray S-receiver functions. Solid Earth, 2015, 6, 957-970.	2.8	20
89	Deep seismic images of the Southern Andes. , 2006, , .		18
90	Details of the Doublet Moho Structure beneath Lhasa, Tibet, Obtained by Comparison of P and S Receiver Functions. Bulletin of the Seismological Society of America, 2011, 101, 1259-1269.	2.3	18

Χιαομυι Υυαν

#	Article	IF	CITATIONS
91	Receiver function images of the base of the lithosphere in the Alboran Sea region. Geophysical Journal International, 2011, 187, 1019-1026.	2.4	18
92	Seismic Evidence for Lateral Asthenospheric Flow Beneath the Northeastern Tibetan Plateau Derived From S Receiver Functions. Geochemistry, Geophysics, Geosystems, 2019, 20, 883-894.	2.5	18
93	Crustal Radial Anisotropy and Linkage to Geodynamic Processes: A Study Based on Seismic Ambient Noise in Southern Madagascar. Journal of Geophysical Research: Solid Earth, 2018, 123, 5130-5146.	3.4	17
94	Mantle Transition Zone Structure Beneath Myanmar and Its Geodynamic Implications. Geochemistry, Geophysics, Geosystems, 2020, 21, e2020GC009262.	2.5	17
95	Double seismic discontinuities at the base of the mantle transition zone near the Mariana slab. Geophysical Research Letters, 2007, 34, .	4.0	16
96	Imaging the Mantle Lithosphere below the China cratons using S-to-p converted waves. Tectonophysics, 2019, 754, 73-79.	2.2	16
97	BRAVOSEIS: Geophysical investigation of rifting and volcanism in the Bransfield strait, Antarctica. Journal of South American Earth Sciences, 2020, 104, 102834.	1.4	16
98	Structure and Stress Field of the Lithosphere Between Pamir and Tarim. Geophysical Research Letters, 2021, 48, e2021GL095413.	4.0	15
99	Seismic structure of the lithosphere beneath <scp>NW</scp> <scp>N</scp> amibia: Impact of the <scp>T</scp> ristan da <scp>C</scp> unha mantle plume. Geochemistry, Geophysics, Geosystems, 2017, 18, 125-141.	2.5	14
100	Seismic Anisotropy Beneath the Pamir and the Hindu Kush: Evidence for Contributions From Crust, Mantle Lithosphere, and Asthenosphere. Journal of Geophysical Research: Solid Earth, 2018, 123, 10,727.	3.4	13
101	De-noising receiver function data using the Seislet Transform. Geophysical Journal International, 2019, 217, 2047-2055.	2.4	13
102	Lateral growth of NE Tibetan Plateau restricted by the Asian lithosphere: Results from a dense seismic profile. Gondwana Research, 2020, 87, 238-247.	6.0	12
103	Crustal Structure of Sri Lanka Derived From Joint Inversion of Surface Wave Dispersion and Receiver Functions Using a Bayesian Approach. Journal of Geophysical Research: Solid Earth, 2020, 125, e2019JB018688.	3.4	12
104	The M w 3.1–4.7 earthquakes in the southern Baltic Sea and adjacent areas in 2000, 2001 and 2004. Journal of Seismology, 2008, 12, 413-429.	1.3	11
105	Tracking unilateral earthquake rupture by P-wave polarization analysis. Geophysical Journal International, 2012, 188, 1141-1153.	2.4	11
106	Connection between the Jurassic oceanic lithosphere of the Gulf of CÃ <sub>i</sub> diz and the Alboran slab imaged by Sp receiver functions. Geology, 2019, 47, 227-230.	4.4	11
107	Shear wave splitting and shear wave splitting tomography of the southern Puna plateau. Geophysical Journal International, 2014, 199, 688-699.	2.4	10
108	Lithospheric Delamination Beneath the Southern Puna Plateau Resolved by Local Earthquake Tomography. Journal of Geophysical Research: Solid Earth, 2020, 125, e2019JB019040.	3.4	9

Χιαοήμι Υμάν

#	Article	IF	CITATIONS
109	Deep Crustal Contact Between the Pamir and Tarim Basin Deduced From Receiver Functions. Geophysical Research Letters, 2021, 48, e2021GL093271.	4.0	9
110	Observations of guided waves from the Pamir seismic zone provide additional evidence for the existence of subducted continental lower crust. Tectonophysics, 2019, 762, 1-16.	2.2	8
111	Impact of the Juan Fernandez Ridge on the Pampean Flat Subduction Inferred From Full Waveform Inversion. Geophysical Research Letters, 2021, 48, e2021GL095509.	4.0	7
112	Moho and uppermost mantle structure in the Alpine area from S-to-P converted waves. Solid Earth, 2021, 12, 2503-2521.	2.8	7
113	Response of mantle transition zone thickness to plume buoyancy flux. Geophysical Journal International, 2010, 180, 49-58.	2.4	6
114	Backâ€Arc Extension of the Central Bransfield Basin Induced by Ridge–Trench Collision: Implications From Ambient Noise Tomography and Stress Field Inversion. Geophysical Research Letters, 2021, 48, e2021GL095032.	4.0	6
115	Seismic Detection and Characterization of the Altiplano-Puna Magma Body, Central Andes. , 2003, , 789-807.		5
116	Tracing the Hawaiian Mantle Plume by Converted Seismic Waves. , 2007, , 49-69.		5
117	Geodynamic processes of the continental deep subduction: Constraints from the fine crustal structure beneath the Pamir plateau. Science China Earth Sciences, 2020, 63, 649-661.	5.2	5
118	Seismic structure across central Myanmar from joint inversion of receiver functions and Rayleigh wave dispersion. Tectonophysics, 2021, 818, 229068.	2.2	5
119	Eastward Dipping Style of the Underthrusting Indian Lithosphere Beneath the Tethyan Himalaya Illuminated by P and S Receiver Functions. Journal of Geophysical Research: Solid Earth, 2021, 126, .	3.4	4
120	Lateral Growth Mechanism of Protoâ€ībetan Plateau in the Late Paleogene: Implications From Detailed Crustal Structures of the Hoh Xil Basin. Geophysical Research Letters, 2022, 49, .	4.0	4
121	Brief communication "Seismic and acoustic-gravity signals from the source of the 2004 Indian Ocean Tsunami". Natural Hazards and Earth System Sciences, 2012, 12, 287-294.	3.6	3
122	Locating the Tohoku-Oki 2011 tsunami source using acoustic–gravity waves. Journal of Seismology, 2012, 16, 215-219.	1.3	3
123	Preservation of the Iberian Tethys paleomargin beneath the eastern Betic mountain range. Gondwana Research, 2022, 106, 237-246.	6.0	3
124	Seismic, Receiver Function Technique. Encyclopedia of Earth Sciences Series, 2011, , 1258-1269.	0.1	2
125	Velocity structure and radial anisotropy of the lithosphere in southern Madagascar from surface wave dispersion. Geophysical Journal International, 2020, 224, 1930-1944.	2.4	2
126	Seismic discontinuities in the lithospheric mantle at the Dead Sea Transform. Geophysical Journal International, 2020, 223, 1948-1955.	2.4	1

Χιαοήμι Υμάν IF ARTICLE CITATIONS Seismic, Receiver Function Technique. Encyclopedia of Earth Sciences Series, 2021, , 1580-1592. Receiver Functions with S Waves., 2016, , 1-16. 128 1 Crustal and uppermost mantle structure of the NW Namibia continental margin and the Walvis Ridge 129 derived from ambient seismic noise. Geophysical Journal International, 2022, 230, 377-391. Moho Doublet in Southern Tibet and Its Tectonic Implication. Acta Geologica Sinica, 2019, 93, 43-44. 130 1.4 0 Seismic imaging of subduction of continental crust beneath the Pamir. Acta Geologica Sinica, 2019, 93, 65-65.

Seismic, Receiver Function Technique. Encyclopedia of Earth Sciences Series, 2019, , 1-13. 132 0.1 0

#